Supplemental Inventory

1. Supplemental figures 1-5
2. Supplemental figure legends
3. Extended experimental procedures
4. Supplemental references

Explanation of supplemental figures:

Figure S1 is related to Figure 1. It includes an inactivated virus as a control for the actual virus and electron microscopy analyses that support the main conclusion that the MNV CR6 virus triggers abnormalities in Paneth cells.

Figure S2 is related to Figure 2. It includes data concerning the replication of the viruses used in the manuscript which are relevant to disease mechanism. It also includes quantification of Paneth cell morphology in the presence of MNV CW3 virus that supports the histology in the main text figure.

Figure S3 is related to Figure 3. This is a heatmap of the genes represented in a subset of the main text figure, genes that display similar changes between genotypes.

Figure S4 is related to Figure 3. This is microarray analyses that adds infection with MNV CW3 as an additional variable to the microarray analyses in the main text figure.

Figure S5 is related to Figures 4, 5, and 6. This is measuring viral replication in the mice that have received similar DSS treatment as the mice from the main text figures.

Figure S1

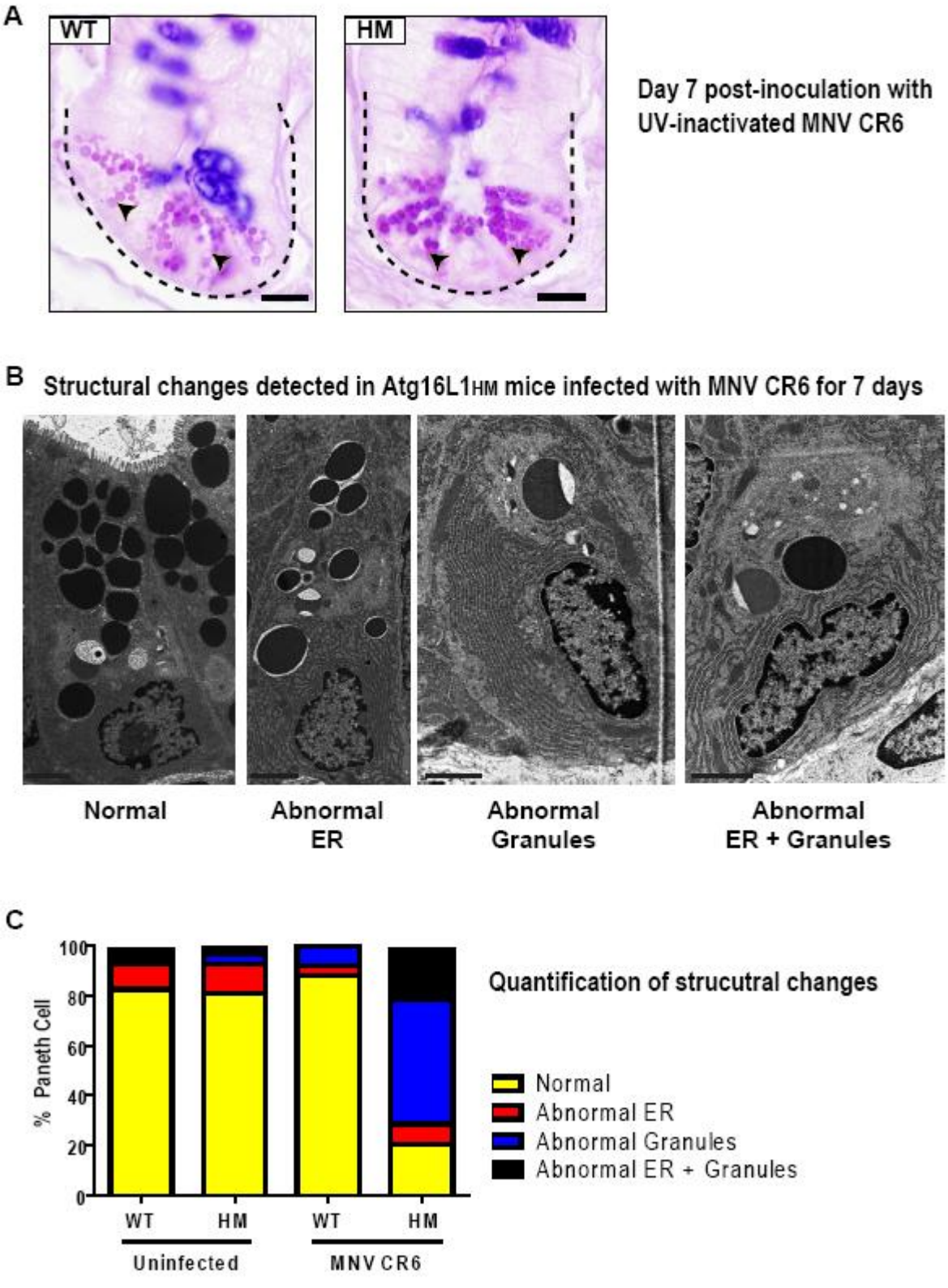
A
WT
HM
Day 7 post-inoculation with
UV-inactivated MNV CR6
B
Structural changes detected in Atg16L1HM mice infected with MNV CR6 for 7 days
Normal
Abnormal ER
Abnormal Granules
Abnormal ER + Granules
C
% Paneth Cell
100
80
60
40
20
0
WT
HM
WT
HM
Uninfected
MNV CR6
Quantification of strucutral changes
Normal
Abnormal ER
Abnormal Granules
Abnormal ER + Granules

Figure S2

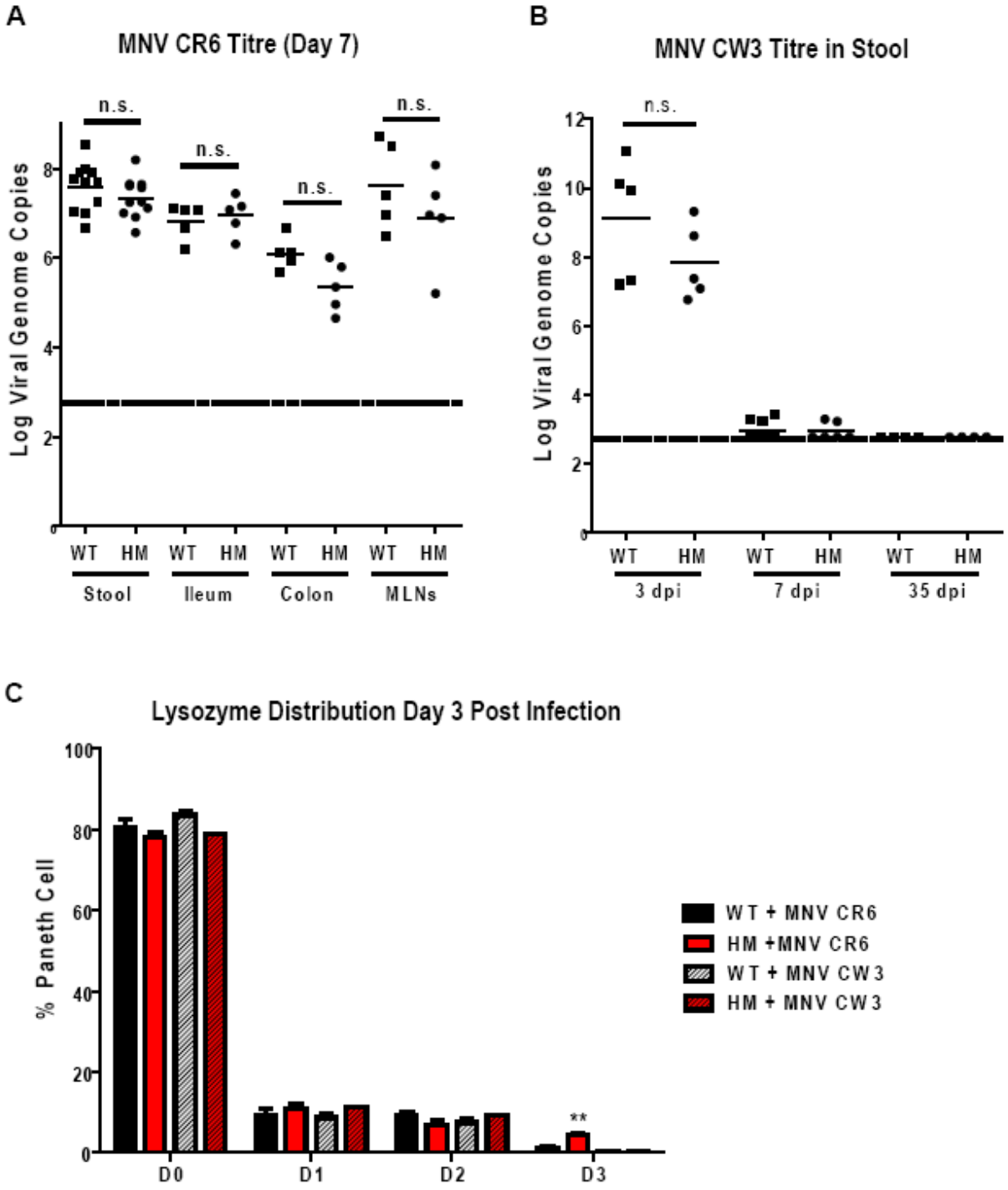
A
MNV CR6 Titre (Day 7)
Log Viral Genome Copies
n.s.
WT HM WT HM WT HM WT HM
Stool
Ileum
Colon
MLNs
B
MNV CW3 Titre in Stool
Log Viral Genome Copies
n.s.
WT HM WT HM WT HM
3 dpi
7 dpi
35 dpi
C
Lysozyme Distribution Day 3 Post Infection
% Paneth Cell
**
D0
D1
D2
D3
WT + MNV CR6
HM +MNV CR6
WT + MNV CW3
HM + MNV CW3

Figure S3

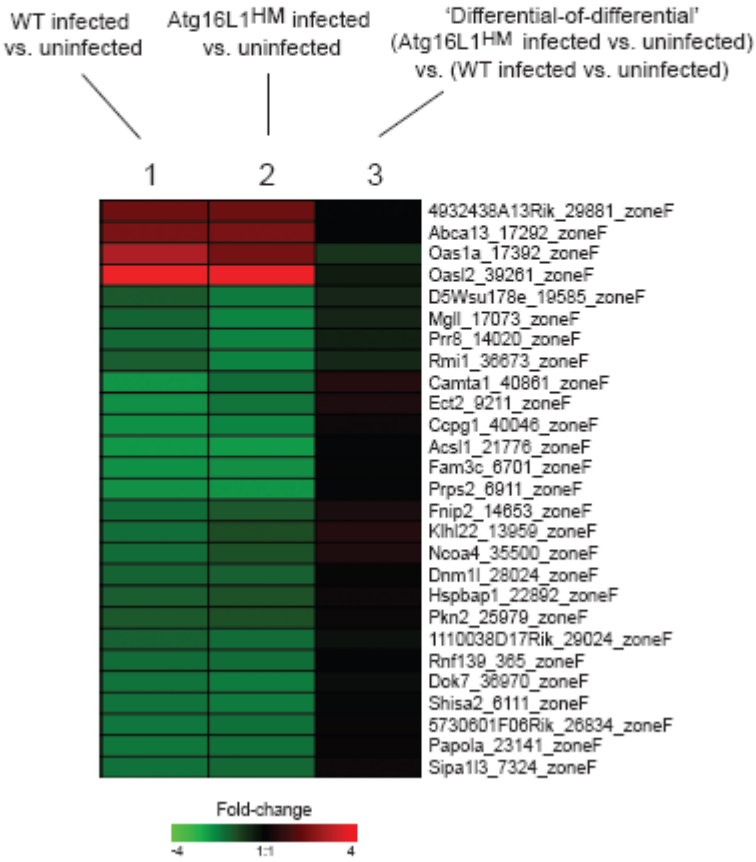
WT infected vs. uninfected
Atg16L1HM infected vs. uninfected
'Differential-of-differential' (Atg16L1HM infected vs. uninfected) vs. (WT infected vs. uninfected)
1
2
3
4932438A13Rik_29881_zoneF
Abca13_17292_zoneF
Oas1a_17392_zoneF
Oasl2_39261_zoneF
D5Wsu178e_19585_zoneF
Mgll_17073_zoneF
Prr8_14020_zoneF
Rmi1_38673_zoneF
Camta1_40861_zoneF
Ect2_9211_zoneF
Ccpg1_40046_zoneF
Acsl1_21776_zoneF
Fam3c_6701_zoneF
Prps2_6911_zoneF
Fnip2_14653_zoneF
Klhl22_13959_zoneF
Ncoa4_35500_zoneF
Dnm1l_28024_zoneF
Hspbap1_22892_zoneF
Pkn2_25979_zoneF
1110038D17Rik_29024_zoneF
Rnf139_365_zoneF
Dok7_36970_zoneF
Shisa2_6111_zoneF
5730601F06Rik_26834_zoneF
Papola_23141_zoneF
Sipa1l3_7324_zoneF
Fold-change
-4
1:1
4

Figure S4

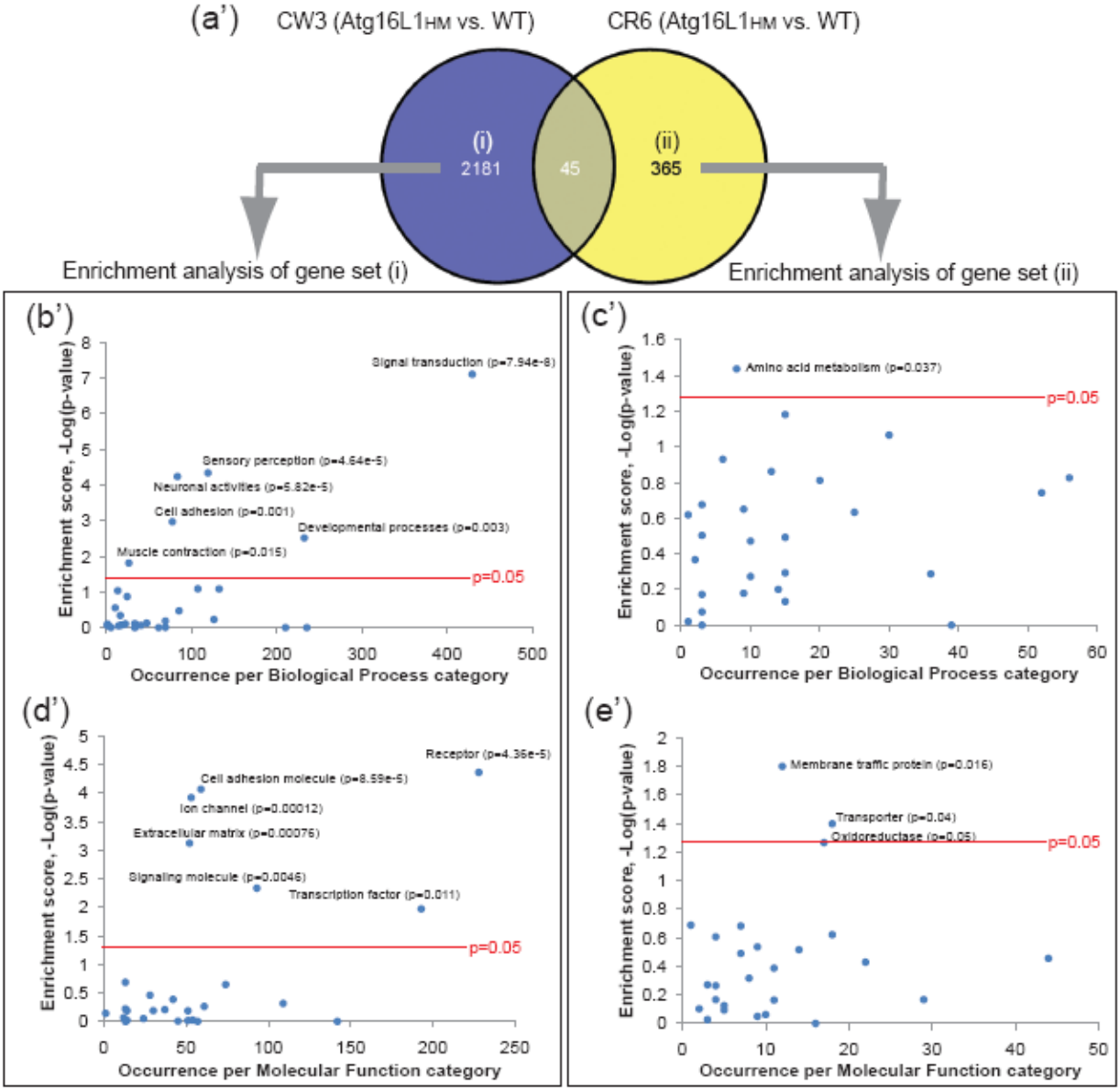
(a')
CW3 (Atg16L1HM vs. WT)
CR6 (Atg16L1HM vs. WT)
(i)
2181
45
(ii)
365
Enrichment analysis of gene set (i)
Enrichment analysis of gene set (ii)
(b')
Enrichment score, -Log(p-value)
Signal transduction (p=7.94e-8)
Sensory perception (p=4.64e-5)
Neuronal activities (p=5.82e-5)
Cell adhesion (p=0.001)
Developmental processes (p=0.003)
Muscle contraction (p=0.015)
p=0.05
Occurrence per Biological Process category
(c')
Enrichment score, -Log(p-value)
Amino acid metabolism (p=0.037)
p=0.05
Occurrence per Biological Process category
(d')
Enrichment score, -Log(p-value)
Receptor (p=4.36e-5)
Cell adhesion molecule (p=8.59e-5)
Ion channel (p=0.00012)
Extracellular matrix (p=0.00076)
Signaling molecule (p=0.0046)
Transcription factor (p=0.011)
p=0.05
Occurrence per Molecular Function category
(e')
Enrichment score, -Log(p-value)
Membrane traffic protein (p=0.016)
Transporter (p=0.04)
Oxidoreductase (p=0.05)
p=0.05
Occurrence per Molecular Function category

Figure S5

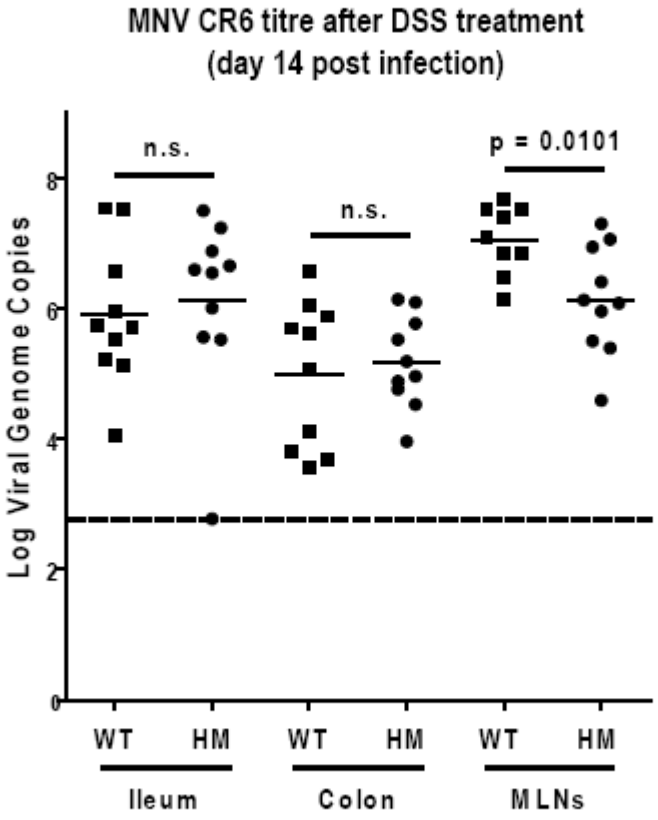
MNV CR6 titre after DSS treatment
(day 14 post infection)
n.s.
n.s.
p = 0.0101
Log Viral Genome Copies
8
6
4
2
0
WT
HM
WT
HM
WT
HM
Ileum
Colon
MLNs

SUPPLEMENTAL FIGURE LEGENDS

Figure S1, related to Figure 1. MNV CR6 infection triggers Paneth cell abnormalities.

(A) Atg16L1^{HM} and WT mice in the enhanced barrier facility were orally inoculated with $3x10^7$ particle forming units (pfu) of MNV CR6 inactivated by UV-irradiation. Ileal sections were stained with PAS-alcian blue to detect Paneth granules by light microscopy (n = 5 mice/genotype). The dotted line denotes crypt unit and arrowheads indicate typical Paneth cell granules. Scale bar represents 10 μm.

(B) Atg16L1^{HM} and WT mice infected with MNV CR6 for 7 days or uninfected were analyzed by transmission electron microscopy (n = 3 mice/condition). Paneth cells were categorized as having a normal appearance, distended endoplasmic reticulum (ER), diminished granules (≤2 granules present), or a combination of these ER and granule defects. Representative images of each category are shown. Bar = 2 μm.

(C) Quantification of the percentage of Paneth cells corresponding to the categories defined in (B).

Figure S2, related to Figure 2. Properties of MNV CR6 and CW3 associated with Paneth cells.

(A) Viral genome copy numbers were determined by qRT-PCR in various tissues harvested from Atg16L1^{HM} and WT mice 7 days after oral inoculation with MNV CR6 (n = 11 mice/genotype). MLNs indicate mesenteric lymph nodes. Dotted line represents a limit of detection of 600 genome copies.

(B) Stool pellets were collected from WT and Atg16L1^{HM} mice 3, 7, and 35 days post oral inoculation with 3x10^{7} pfu MNV CW3. Viral genome copy numbers were determined by qRT-PCR (n = 5 mice/genotype for day 3 and day 7 samples, n = 4 mice/genotype for day 35 samples). Dotted line represents a limit of detection of 600 genome copies.

(C) Atg16L1^{HM} and WT mice infected with 3x10^{7} pfu of either MNV CR6 or MNV CW3 for 3 days. The percentage of Paneth cells displaying each of the four types of lysozyme distribution patterns were quantified (n = 3 mice/condition, mean +/-SEM). A slight increase in the D3 population was detected in Atg16L1^{HM} compared to WT mice infected with MNV CR6 ($p = 0.069$), but otherwise Paneth cells were similar to uninfected WT mice (Figure 1D). No granule abnormalities were detected by light microscopy in these conditions (n = 4 mice/genotype, not shown).

Figure S3, related to Figure 3. Genes that display similar changes in expression in Paneth cells from WT and *Atg16L1* mutant mice in response to MNV CR6.

Heatmap of genes represented in Zone F of the Venn diagram from Figure 3. Changes in gene expression within each comparison are represented as Log_2-transformed fold-changes ($p < 0.05$, fold-change > 1.5).

Figure S4, related to Figure 3. Comparison of gene expression changes in response to MNV CR6 versus CW3.

Comparison of respective genes that were altered in mRNA abundance in Atg16L1^{HM} versus WT mice infected with MNV CW3 (i) and MNV CR6 (ii) is illustrated by the Venn

diagram ($p < 0.05$, fold-change >1.5) (a'). A significant enrichment of the biological processes categories of signal transduction, sensory perception, neuronal activities, cell adhesion, developmental processes, and muscle contraction was observed among genes uniquely differentially expressed when infected with MNV CW3 (b'). This is distinct from infection with MNV CR6 which showed enrichment for amino acid metabolism among the differentially expressed genes (c'). A significant enrichment of the molecular functions categories receptor, cell adhesion, ion channel, extracellular matrix, signaling molecule, and transcription factor was observed in Atg16L1^{HM} versus WT mice infected with MNV CW3 (d'). In contrast, membrane traffic protein and transporter were associated with MNV CR6 and not MNV CW3 (e').

Figure S5, related to Figures 4, 5, and 6. MNV CR6 replication is similar in WT and Atg16L1^{HM} mice treated with DSS.

Ileum, colon, and mesenteric lymph nodes (MLNs) were harvested from WT and Atg16L1^{HM} mice orally inoculated with $3x10^7$ pfu of MNV CR6 for 7 days prior to receiving DSS for another week. Viral genome copy numbers were determined in these tissues by qRT-PCR (n = 10 mice/genotype). Dotted line represents a limit of detection of 600 genome copies.

EXTENDED EXPERIMENTAL PROCEDURES

Administration of DSS

Aqueous solution of DSS (TDB Consultancy, Uppsala, Sweden) was filtered using a 0.22-μm cellulose acetate filter prior to administration through drinking water. For

antibiotics experiments, 1 g/L ampicillin (Columbus Serum Company, Columbus, OH), 500 mg/L vancomycin (Sigma, St. Louis, MO), 1 g/L neomycin sulfate (Sigma, St. Louis, MO), and 1 g/L metronidazole (Sigma, St. Louis, MO) were dissolved in drinking water along with 2.5% DSS, then filtered using a 0.22-μm cellulose acetate filter. 20 mg/ml sugar-sweetened grape Kool-Aid Mix (Kraft Foods) was included in the water to encourage consumption. All mice receiving antibiotics displayed a similar degree of focal ulceration in the descending colon compared to mice receiving DSS alone, indicating that the presence of antibiotics did not interfere with the administration of DSS through water and that bacteria are not essential for this aspect of DSS-induced intestinal injury. Additionally, both WT and Atg16L1^{HM} mice displayed epithelial hypo-proliferation in non-ulcerated regions of the rectum that is similar to findings in DSS-treated germ-free mice (Pull et al., 2005), thus confirming successful antibiotic uptake. For TNFα neutralization, mice received 1 mg of either hamster anti-TNFα (TN3–19.12) or hamster anti-PIP isotype control antibodies 1 day prior to DSS treatment, then received a second injection of 0.5 mg 5 days later (4 days into DSS treatment). For IFNγ neutralization, mice received one injection of 0.2 mg of hamster anti-IFNγ (H22) 1 day prior to DSS treatment. Blocking antibodies were kindly provided by Dr. Robert Schreiber (Sheehan et al., 1989; Schreiber et al., 1985).

UV inactivation of MNV CR6

UV-inactivated virus was generated by placing 600 μl of 1.2x10^9 pfu/ml MNV CR6 in a 6 well plate and subjected to 1000 mJ of UV in a UV Stratalinker 2400 (Stratagene). The

inactivation was confirmed by qRT-PCR for the presence of viral genome in stool specimens 7 days post infection.

Microscopy

The distal ileum and colon were removed, cut open along the length, and pinned on black wax. The ileum was fixed in 10% formalin and the colon was fixed in Bouin's fixative overnight at 4^{o}C. 2 cm strips of intestinal tissues were embedded in agar to enrich for well-oriented crypt-villus units. To determine villus blunting, villus height was quantified in ileal sections that were cut perpendicular to the villus-crypt axis as defined by the presence of a visible crypt lumen from the orifice to the base of the crypt, thereby minimizing tissue orientation-based artifacts of villus height measurements (Stappenbeck et al., 2003). Images were taken on an Olympus BX51 microscope. Immunohistochemistry for lysozyme was previously described (Cadwell et al., 2008). Sections were viewed with a Zeiss Axiovert 200 inverted fluorescence microscope and quantified on an Olympus AX70 epi-fluorescence microscope. Electron microscopy of ileal crypts was previously described (Cadwell et al., 2008).

Laser Capture Microdissection

The distal ileum was removed, cut open along the length, pinned on black wax, and fixed in methacarn. The tissue was blocked and embedded as described above and 0.6 μm serial sections were cut and deparaffinized. The crypt-base epithelial cells enriched for Paneth cells were captured and RNA was isolated by previously described techniques (Stappenbeck et al., 2003; Pull et al., 2005). 25 ng of total RNA from each

sample was amplified using the Transplex Complete Whole Transcriptome Amplification Kit (Sigma, St Louis MO), labeled using a modified protocol with the ULS aRNA Fluorescent Cy5 labeling kit (Kreatech Diagnostics, The Netherlands); and purified using DNA Clean and Concentrate spin columns according to manufacturer's protocol (Zymo Research Corporation, Orange CA).

Microarray

cDNA was hybridized to 4x44K Mouse Whole Genome Microarrays (Agilent) for 18 hours following the manufacturer's protocol. Microarrays were washed in 0.01x SSC/0.005% Triton X-102 at 40ºC, dried with HEPA filtered compressed nitrogen and scanned on an Agilent Technologies DNA Microarray Scanner at 5 μm resolution. Data were extracted from the scanned image using Agilent Technologies Feature Extraction Software, background subtracted, and normalized by the Lowess method (Yang et al., 2002). CEL files have been submitted to Array Express, accession numbers E-TABM-957 (WT + MNV CR6 and Atg16L1^{HM} + MNV CR6) and E-TABM-958 (WT uninfected, Atg16L1^{HM} uninfected, WT + MNV CW3, and Atg16L1^{HM} + MNV CW3). A factorial design approach (Scholtens et. al., 2004) was implemented in the R programming language, in which a linear model (Smyth, 2005) was fit with a coefficient for each of the 4 factor combinations and then simultaneously extracted as contrasts for each of the three comparisons (summarized in the Venn diagram of Figure 3) including the interaction ('differential-of-differential') term. Sets of differentially expressed genes ($p < 0.05$ and fold-change >1.5) for each comparison were examined for enrichment in terms of biological process or molecular function categories compared to their representation

in the whole genome using the Panther classification system (Mi et al., 2007). Enrichment p-values were computed using the hypergeometric distribution and implemented in the R language.

SUPPLEMENTAL REFERENCES

Cadwell,K., Liu,J.Y., Brown,S.L., Miyoshi,H., Loh,J., Lennerz,J.K., Kishi,C., Kc,W., Carrero,J.A., Hunt,S., Stone,C.D., Brunt,E.M., Xavier,R.J., Sleckman,B.P., Li,E., Mizushima,N., Stappenbeck,T.S., and Virgin,H.W. (2008). A key role for autophagy and the autophagy gene Atg16l1 in mouse and human intestinal Paneth cells. Nature *456*, 259-263.

Mi,H., Guo,N., Kejariwal,A., and Thomas,P.D. (2007). PANTHER version 6: protein sequence and function evolution data with expanded representation of biological pathways. Nucleic. Acids Res. *35*, D247-D252.

Pull,S.L., Doherty,J.M., Mills,J.C., Gordon,J.I., and Stappenbeck,T.S. (2005). Activated macrophages are an adaptive element of the colonic epithelial progenitor niche necessary for regenerative responses to injury. Proc Natl Acad Sci U. S. A *102*, 99-104.

Scholtens D, Miron A, Merchant FM, Miller A, Miron PL, Iglehart JD, Gentleman R. (2004). Analyzing Factorial Designed Microarray Experiments. Journal of Multivariate Analysis. 90:19-43.

Schreiber,R.D., Hicks,L.J., Celada,A., Buchmeier,N.A., and Gray,P.W. (1985). Monoclonal antibodies to murine gamma interferon which differentially modulate macrophage activation and antiviral activity. J. Immunol. *134*, 1609-1618.

Sheehan,K.C., Ruddle,N.H., and Schreiber,R.D. (1989). Generation and characterization of hamster monoclonal antibodies that neutralize murine tumor necrosis factors. J. Immunol. *142*, 3884-3893.

Smyth, G. K. (2005). Limma: linear models for microarray data. In Bioinformatics and Computational Biology Solutions using R and Bioconductor. R. Gentleman, V. Carey, S. Dudoit, R. Irizarry, W. Huber, ed. (Springer, New York).

Stappenbeck,T.S., Mills,J.C., and Gordon,J.I. (2003). Molecular features of adult mouse small intestinal epithelial progenitors. Proc Natl Acad Sci U. S. A *100*, 1004-1009.

Yang,Y.H., Dudoit,S., Luu,P., Lin,D.M., Peng,V., Ngai,J., and Speed,T.P. (2002). Normalization for cDNA microarray data: a robust composite method addressing single and multiple slide systematic variation. Nucleic Acids Res. *30*.